# University of Groningen

## Bioinspired Processing

Khoonkari, Mohammad; Sayed, Julien Es; Oggioni, Marta; Amirsadeghi, Armin; Parisi, Daniele; Kruyt, Frank; Rijn, Patrick van; Włodarczyk-Biegun, Małgorzata Katarzyna; Kamperman, Marleen

**IMPORTANT NOTE: You are advised to consult the publisher's version (publisher's PDF) if you wish to cite from it. Please check the document version below.**

*Document Version*
Publisher's PDF, also known as Version of record

[Link to publication in University of Groningen/UMCG research database](#)

# Bioinspired Processing: Complex Coacervates as Versatile Inks for 3D Bioprinting

Mohammad Khoonkari, Julien Es Sayed,* Marta Oggioni, Armin Amirsadeghi,
Peter Dijkstra, Daniele Parisi, Frank Kruyt, Patrick van Rijn,
Małgorzata Katarzyna Włodarczyk-Biegun,* and Marleen Kamperman*

3D bioprinting is a powerful fabrication technique in biomedical engineering, which is currently limited by the number of available materials that meet all physicochemical and cytocompatibility requirements for biomaterial inks. Inspired by the key role of coacervation in the extrusion and spinning of many natural materials, hyaluronic acid–chitosan complex coacervates are proposed here as tunable biomaterial inks. Complex coacervates are obtained through an associative liquid–liquid phase separation driven by electrostatic attraction between oppositely charged macromolecules. They offer bioactive properties and facile modulation of their mechanical properties through mild physicochemical changes in the environment, making them attractive for 3D bioprinting. Fine-tuning the salt concentration, pH, and molecular weight of the constituent polymers results in biomaterial inks that are printable in air and water. The biomaterial ink, initially a viscoelastic fluid, transitions into a viscoelastic solid upon printing due to dehydration (for printing in air) or due to a change in pH and ionic composition (for printing in solution). Consequently, scaffolds printed using the complex coacervate inks are stable without the need for post-printing processing. Fabricated cell culture scaffolds are cytocompatible and show long-term topological stability. These results pave the way to a new class of easy-to-handle tunable biomaterials for biofabrication.

## 1. Introduction

3D bioprinting is a powerful technique to construct complex 3D architectures that mimic the hierarchical organization of native tissues. Such structures find application as advanced 3D cell culture substrates or tissue models and hold promise for personalized implants.[1] During the bioprinting process, the biomaterial ink is typically extruded through a nozzle as a viscous liquid that is made to solidify immediately after deposition to maintain the 3D shape.[2] Therefore, adequate rheological characteristics are key requirements for a practical biomaterial ink, next to cytocompatibility.[3] To comply with these requirements, biomaterial inks are most often composed of water-soluble polymer precursors dissolved in (a large amount of) water. Colloidal dispersions of jammed swollen microgels and entangled cellulose nanofibers have also recently been shown to exhibit suitable rheological behavior to be used as biomaterial ink.[4–7] Yet, the paradox of this approach is that the essential water-solubility of the precursors also threatens the (long-term) structural integrity and stability of the printed structures in the wet conditions that are typical for biomedical applications. To prevent disintegration

M. Khoonkari, J. Es Sayed, M. Oggioni, A. Amirsadeghi, P. Dijkstra,
M. K. Włodarczyk-Biegun, M. Kamperman
Zernike Institute for Advanced Materials
University of Groningen
Nijenborgh 4, Groningen 9747 AG, The Netherlands
E-mail: j.s.es.sayed@rug.nl; marleen.kamperman@rug.nl

M. Khoonkari, F. Kruyt
Department of Medical Oncology
University of Groningen
University Medical Center Groningen
Hanzeplein 1, Groningen 9713 GZ, The Netherlands

D. Parisi
Engineering and Technology Institute Groningen (ENTEG)
University of Groningen
Nijenborgh 4, Groningen9747 AG, The Netherlands

P. van Rijn
Department of Biomedical Engineering-FB40
University of Groningen
University Medical Center Groningen
A. Deusinglaan 1, Groningen9713 AV, The Netherlands

M. K. Włodarczyk-Biegun
Biotechnology Centre
The Silesian University of Technology
Bolesława Krzywoustego 8, Gliwice 44-100, Poland
E-mail: malgorzata.wlodarczyk-biegun@polsl.pl

of the printed structures and dissolution of the water-soluble polymers in the culture medium or body fluids, the polymer precursors are therefore crosslinked, typically post-printing.[8,9] This can be achieved by chemical means, via strong covalent bonds between the polymer chains or by physical means, via association of "stickers" attached to the polymer chains (host-guest, metal–ligand, and hydrophobic interactions).[10–13] However, for both crosslinking strategies, a chemical modification of the polymer precursors prior to printing, or a post-printing treatment such as UV curing or calcium ions (Ca$^{2+}$) addition, or both, are necessary.[14] This crosslinking not only limits the ease of preparation and application of the biomaterial inks, but may also cause cytotoxic effects when the system contains unreacted adhesive, catalyst, or initiator residues.[11,15–17]

Remarkably, the technological challenges involved in designing an aqueous-based biomaterial ink that is chemically and structurally stable with a minimal need for pre- or post-printing processing have already been overcome by many natural organisms. Spiders and velvet worms are able to produce strong and tough fibers that originate as fluid globules containing a high concentration of proteins.[18–20] In underwater conditions, caddisfly larvae and sandcastle worms secrete fluid, water-insoluble proteinaceous adhesive material that quickly solidifies when in contact with seawater.[21,22] Recently, it was discovered that these organisms use coacervate phases as intermediates toward the final material.[18–21] Coacervation is defined as a liquid–liquid phase separation, often driven by electrostatic and/or hydrophobic interactions, resulting in a dense polymer-rich phase (the coacervate) in equilibrium with a dilute phase containing mainly water (the supernatant). When coacervation is caused by the interaction of two oppositely charged polymers, it is referred to as complex coacervation.[23,24] In this scenario, the polymers are both hydrophilic and water soluble, but upon mixing, phase separation occurs in which a complex coacervate is formed that is immiscible with the surrounding aqueous environment. This process makes coacervates very suitable as biomaterial inks, as the immiscibility ensures stability of the printed scaffolds in a water environment.

Both natural oppositely charged polyelectrolyte couples such as polysaccharides like alginate,[25] hyaluronic acid and chitosan,[26] carrageenan,[27] and proteins such as gelatin,[25] lysozyme,[28] and synthetic ones have been successfully associated into complex coacervates.[29] For a given polyelectrolyte couple, depending on the salt concentration in the medium, a complex coacervate either behaves as a free-flowing viscoelastic fluid or a rigid polyelectrolyte complex, or anything in between.[30,31] It has also been shown that the pH at which coacervation takes place and the molecular weight ($M_w$) of the oppositely charged polymers can directly influence the viscoelastic properties of the coacervate phase through modification of the strength and dynamics of the non-covalent interactions (i.e., electrostatic, hydrophobic, H-bonding, and entanglements).[23,29]

This tunability of the viscoelastic properties of complex coacervates greatly facilitates aqueous processing of polyelectrolyte materials, as was recently shown for several applications: 1) Complex coacervates were processed into rods and fibers by extrusion and (electro)spinning.[32,33] The associative interactions between the polymer chains enabled successful electrospinning even of very short polymeric chains.[34] Self-coacervated molecularly en-

gineered proteins were also shown to form fibers upon drawing in a similar extrusion process as performed by spiders.[18] 2) Complex coacervates or proto-coacervates (precursor solution in which polyelectrolytes are not interacting yet) were used as injectable underwater adhesives. The fluid character of the complex coacervate allowed precise and spatially controlled material delivery. After delivery, the adhesive transitioned into a solid upon a change in temperature, pH or salt concentration of the environment. Due to the complex coacervate nature of the adhesive, the material remained at the application site during solidification even when fully submerged in water.[35–38] 3) Nano- to microporous filtration membranes were prepared from polyelectrolyte complexes by first casting a homogeneous solution of oppositely charged polyelectrolytes with attractive interactions screened due to the high salt concentration, followed by immersion in salt-free water to induce aqueous phase separation through salt diffusion from the membrane into the bath.[39]

In this work, we exploit the tunable properties of complex coacervates to establish a new class of biomaterial inks. The complex-coacervate-based biomaterial ink developed here is made of two bio-polyelectrolytes, namely hyaluronic acid (HA) and chitosan (CHI). The negatively charged HA is part of almost all tissue types and particularly abundant in soft tissues such as brain, lung, and breast.[40,41] The positively charged CHI is known to facilitate cell adhesion and to promote cytocompatibility.[42] In addition, cytocompatibility of HA/CHI hydrogels was systematically investigated in previous studies.[43,44] Here, we investigated how salt concentration, pH, and $M_w$ affect the rheological properties of the HA–CHI complex coacervates. This way, the optimal formulation was identified for printing HA–CHI complex coacervates with shape stability after deposition without the need of any chemical modification or post-printing processing. Furthermore, we show that printing directly into a phosphate buffered saline (1×-PBS) bath at physiological pH broadens the range of ink formulations that can be successfully printed and results in microporous scaffolds. Finally, high viability of cells cultured on the printed scaffolds is reported, showcasing the potential of complex-coacervate-based inks for biomedical applications.

## 2. Results and Discussions

### 2.1. HA–CHI Complex Coacervates Formation and Viscoelastic Properties

Complex coacervates were formed upon mixing HA and CHI solutions, subsequently separated from the supernatant by centrifugation and used as an ink (**Figure 1**A). The polyelectrolyte solutions consisted of HA chains with an average molecular weight of 30–50 kg mol$^{-1}$ or 200–400 kg mol$^{-1}$, further described as "low $M_w$" and "high $M_w$", respectively, and CHI chains with an average molecular weight of 30 kg mol$^{-1}$, further described as "low $M_w$". An equal number of chargeable monomer units (0.012 M) of both polyelectrolytes was targeted (see Table S1, Supporting Information). The concentration of added NaCl was varied from 0.05 to 0.25 M, and the pH from 5 to 6. These specific pH values were chosen to ensure an ionization degree of both polymers above 75%, as the apparent p$K_a$s of HA and CHI were determined to be 2.2 and 6.5, respectively (see Figure S1A–C,
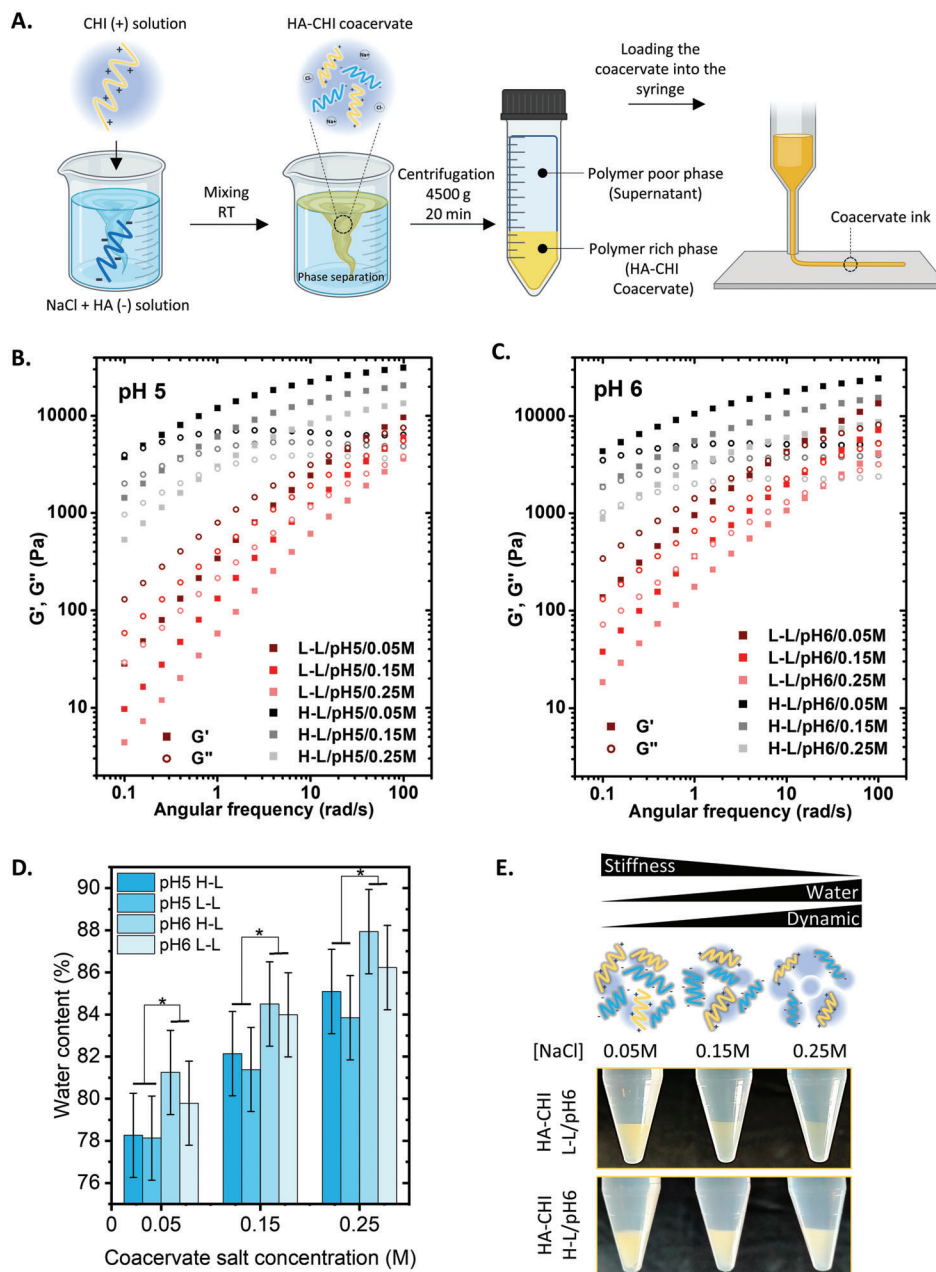
**Figure 1.** Formation of the HA–CHI complex coacervates and their viscoelastic properties and water content. A) Schematic representation of the preparation of printable HA–CHI complex coacervates. Upon mixing HA and CHI at a controlled pH, $M_w$ of the chains and salinity, liquid–liquid phase separation occurs. After centrifugation, the complex coacervate is loaded in a syringe and printed via extrusion. B,C) Frequency sweep data for complex coacervates formed at different salt concentrations and HA-$M_w$ at pH 5 and 6 (at a strain $\gamma = 1\%$). D) Water content of the developed HA–CHI complex coacervates obtained by gravimetric measurements. A significant difference in statistics was considered as $^*p \leq 0.05$. E) Pictures of the centrifuged mixtures showing the HA–CHI complex coacervates, with high and low $M_w$ of HA, formed at pH 5 and 6 and with added NaCl concentrations of 0.05, 0.15, and 0.25 M.

Supporting Information). The salt concentration range investigated was selected to be close to the salinity of physiological medium (0.13 M NaCl as the main component). It is worth noting that the concentration of salt added through the adjustment of the pH is negligible compared to the added NaCl concentration. In this way, a large enough number of electrostatic interactions and a high yield of coacervation was obtained at close-to-physiological conditions. The studied complex coacervate ink formulations are abbreviated as follows: [$M_w$ of HA-$M_w$ of CHI]/pH/[salt concentration], where "H" stands for high $M_w$, and "L" for low $M_w$. As an example H-L/pH6/0.15 M stands for the mix of high $M_w$ HA and low $M_w$ CHI, at pH 6 and an added NaCl concentration of 0.15 M.

To determine the optimal composition for printing, the water content and the rheological properties of the complex coacervate inks were investigated. The effect of the salt concentration

**ADVANCED
SCIENCE NEWS**

www.advancedsciencenews.com

**ADVANCED
MATERIALS**

www.advmat.de

on the rheological properties of the complex coacervates is presented in Figure 1B,C. All the complex coacervates showed a typical response of viscoelastic liquids, with the loss modulus ($G''$) exceeding the storage modulus ($G'$) at low frequencies. The inverse of the $G'$ and $G''$ crossover frequency represents the terminal relaxation time of the system. This indicates the time scale above which the system starts to flow. Regardless of the pH and the $M_w$, it was observed that the crossover frequency increased (i.e., the relaxation time decreased) with increasing salt concentration of the system. In parallel, the moduli values related to the stiffness of the material were found to decrease with increasing salt concentration. Another consequence of the increasing salt concentration is an increase of the water content in the complex coacervates (81–88% for the samples containing high $M_w$ HA at pH 6), and, thus, a lower polymer content as revealed by gravimetric measurements (Figure 1D). The lower polymer density of the complex coacervates upon increasing the salt concentration can also be qualitatively identified in the pictures shown in Figure 1E as an increase in material transparency is observed. These results can all be attributed to the salt plasticization effect of complex coacervates: the increased salt concentration decreases the driving force for polyelectrolyte association that is a combination of Coulombic attraction and entropic gain through counterion release.[23,45–48] The following picture can be drawn: upon increasing the salt concentration, the density of ion pairing between salt ions and polymer increases while the density of electrostatic associations between HA and CHI chains inside the material is decreased. Consequently, as the density of salt ion–polymer increases, more and more polyelectrolytes segments are free to move.

In addition to the effect of salt, we investigated the effect of $M_w$ of HA on the water content and the rheological properties of the resulting HA–CHI complex coacervates. Complex coacervates comprising CHI chains with a $M_w$ of 30 kg mol$^{-1}$ and HA chains with a $M_w$ of 30–50 or 200–400 kg mol$^{-1}$ were formed at fixed pH and salt concentration. In contrast to the effect of salt, the water content of the samples remained unchanged regardless of the $M_w$ (Figure 1D). Meanwhile, when increasing the $M_w$ of the HA chains, the dynamics of the resulting complex coacervates were drastically slowed down, for all investigated pH values and salinity conditions (Figure 1B,C). Regardless of the pH, all complex coacervates formulated with high $M_w$ HA chains exhibited a crossover frequency below 1 rad s$^{-1}$ while the ones formulated with low $M_w$ HA chains showed a crossover frequency above 10 rad s$^{-1}$. Our observations are corroborated by recent studies from Liu et al. and Yu et al.[45,46] Both studies suggest that, in addition to electrostatic interactions, longer chains promote entanglements, adding in fact an additional relaxation mode (reptation) to the complex coacervates, resulting in slower dynamics.

Finally, we assessed the effect of pH at which the HA–CHI complex coacervates were prepared. Interestingly, the water content of the samples prepared at pH 6 are consistently higher than the ones prepared at pH 5 (Figure 1D). This observation can be explained by a combination of a so-called overcharging effect of the complex coacervate that occurs when positive and negative charges present on polymer chains are not balanced, and by the reduced charge density on the CHI chains.[48] When forming complex coacervates, HA and CHI were mixed at 1:1 ratio of chargeable monomer units regardless of the pH. From the

curves obtained by titration and degree of ionization presented in Figure S1A,B (Supporting Information), at pH 5 both HA and CHI are expected to be fully charged and to fully compensate upon complexation. At pH 6, only ≈78% of the chargeable amine units of the CHI are positively charged and total charge compensation is not obtained (Figure S1C, Supporting Information). Zeta potential measurements performed on the supernatant of the centrifuged complex coacervates L-L/pH5/0.05 м and L-L/pH6/0.05 м support the hypothesis of an excess of negative charges, originating from HA, in the medium at pH 6 (Figure S2, Supporting Information). Usually, a higher water content in complex coacervate systems is accompanied by faster relaxation dynamics, for example, as observed at increased salt concentrations. However, despite the higher water content, the dynamics of the complex coacervate samples at pH 6 were significantly slowed down compared to pH 5 (Figure 1B,C). This trend can be explained by the relatively poor solubility of chitosan in water. As the pH increases toward the apparent $pK_a$ of the CHI chains, the increased density of deprotonated amine moieties is expected to increase intra- and interchains hydrogen bonds.[42,49] As a result, the rheological properties are not only a function of the associative phase separation process between HA and CHI through Coulombic interactions and entropic gain from counterion release, but also of the segregative phase separation of CHI and water. Our interpretation is supported by a recent set of studies by Li et al.,[47] Lappan et al.,[50] and Tekaat et al.,[51] who showed by rheology and electron paramagnetic resonance spectroscopy experiments that polyelectrolyte complexes (PECs) formed with poly(acrylic acid) (PAA), combined either with poly(allylamine) (PAH) or poly(diallyldimethyl ammonium chloride) (PDADMAc) at acidic pH, close to PAA's apparent $pK_a$, also exhibit slow dynamics. The authors relate the slow dynamics to the formation of hydrophobic or hydrogen bonded domains of PAA at low degrees of ionization (i.e., at pH $\leq pK_a$s $_{app}$). These examples, as well as recent work from Sun et al. on HA–CHI complex coacervate systems suggest that solvent–polymer interactions are at least as important as salt concentration and $M_w$ for the rheological behavior of a complex coacervate formulation.[52] In the present study, the relative insolubility of the CHI chains in water can be turned into an advantage to develop 3D printable HA–CHI complex coacervates, as will be discussed later.

To conclude, pH, $M_w$, and salinity represent three parameters that can be used to tune the rheological properties of HA–CHI complex coacervates. The following trends were observed: a higher salt concentration, a lower $M_w$, and a lower pH led to faster relaxation of the resulting complex coacervates (Figure 1E,D).

## 2.2. Screening the Shape Fidelity of the HA–CHI Complex-Coacervate-Based Ink

Subsequently, the different complex coacervate formulations were 3D printed and their shape fidelity was visually assessed. **Figure 2**A,B shows images of the printed 2 mm × 2 mm square-mesh scaffolds consisting of 4 layers, using the L-L and the H-L $M_w$ systems, respectively. Image analysis was performed on images of the printed scaffolds, from which a "printability parameter" value (Pr) was calculated as an indicator of the shape fidelity following the protocol proposed by Ouyang et al. (Figure 2C; see

**ADVANCED**
SCIENCE NEWS

www.advancedsciencenews.com

**ADVANCED**
**MATERIALS**

www.advmat.de
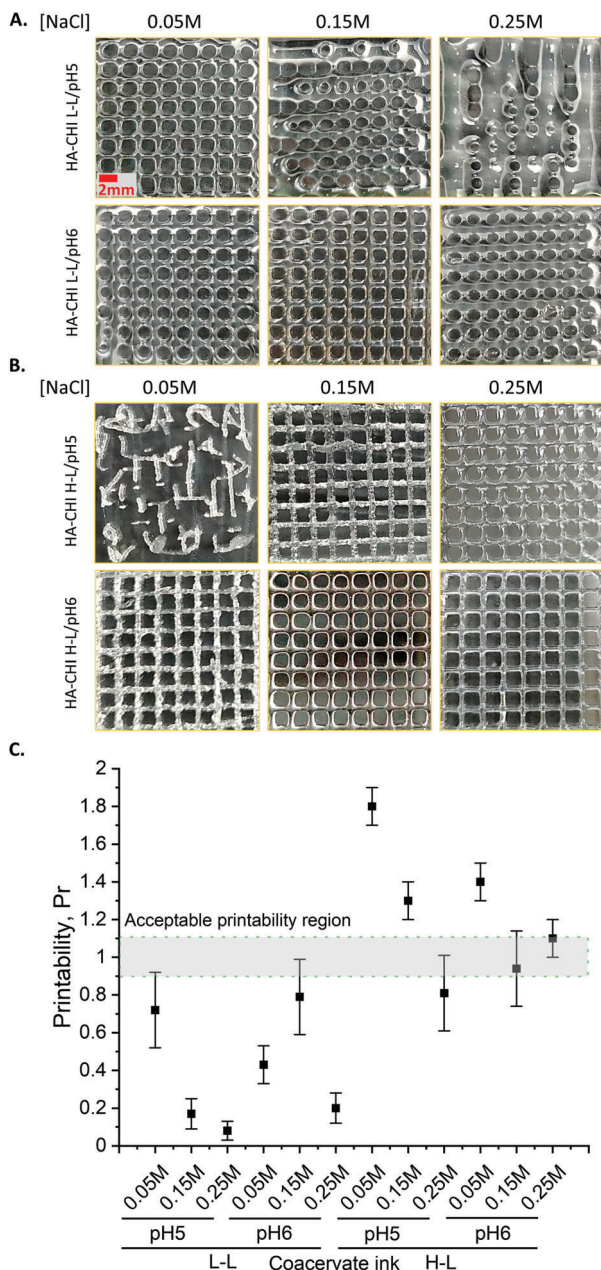
**Figure 2.** Screening the shape fidelity of the HA–CHI complex-coacervate-based inks. A,B) Pictures of 4-layer 2 mm x 2 mm square mesh scaffolds within 1 min after printing obtained using HA–CHI complex-coacervate formulations at 0.05–0.25 M NaCl, pH 5 and 6 with low $M_w$ HA and CHI (L-L) (A) and high $M_w$ HA and low $M_w$ CH (H-L) (B). Scale bar: 2 mm. C) Average "printability parameter" value, Pr, for each of the complex coacervate formulations investigated. The Pr value calculation details can be found in Supporting Information.
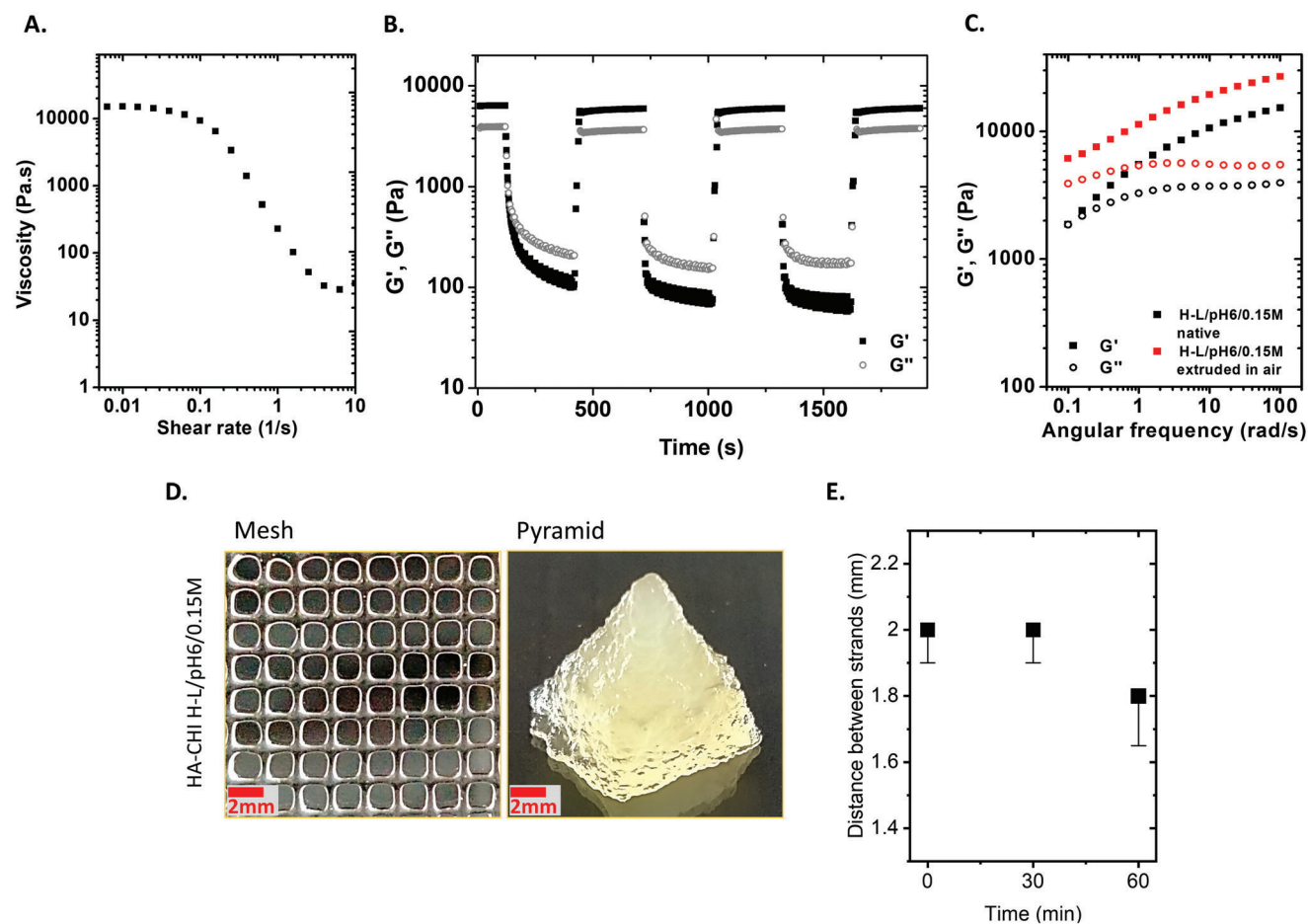
Supporting Information for more information about the image analysis procedure).[9] An ideal square shape results in a Pr value of 1 and deviations from the square geometry result in numbers above or below 1. From this, the H-L/pH6/0.15 M and H-L/pH6/0.25 M samples were identified as the samples with the highest fidelity to the targeted design with an average Pr value

between 0.9 and 1.1. It is interesting to note that these two samples exhibit relatively short characteristic relaxation times, that is, in the order of 30 s, indicating that quickly after printing, shape relaxation is expected. Apparently, in this time scale, dehydration of the thin printed strands becomes a critical parameter that cannot be overlooked. A better understanding of the underlying additional stabilization mechanism caused by dehydration will be discussed in the following section. In contrast, the samples L-L/pH5/0.15 M, L-L/pH5/0.25 M, and L-L/pH6/0.25 M (Figure 2A) all exhibited a very low average Pr value, that is, Pr < 0.2, as the targeted square mesh geometry could not be retained and immediately transitioned into a smooth spherical shape after extrusion. This fast and spontaneous shape relaxation can be directly correlated to the short characteristic relaxation times determined to be below 2 s for these three formulations. The shape fidelity of the printed scaffolds improved when the salinity decreased from 0.25 to 0.05 M and the pH increased from 5 to 6 with average Pr values spanning from 0.4 to 1.3, in direct relation with the slowdown of the dynamics observed in rheological investigation. Finally, formulations made with high $M_w$ HA and low added NaCl concentration of 0.05 M either showed a ragged structure (H-L/pH6/0.05 M) or did not even exhibit any discernable square mesh (H-L/pH5/0.05 M). This over-gelled aspect of the samples is reflected in the high average Pr values measured, that is, Pr > 1.4. In that case, instead of flowing continuously through the nozzle upon extrusion, the material broke due to its rigid and brittle nature as the viscous contribution was much smaller compared to the elastic one. In conclusion, the extrudability and shape fidelity of complex coacervates are closely connected to the strength and the dynamics of the interactions in the system. Samples that are relaxing too fast (on the order of few seconds) or that are too brittle revealed to be poorly printable.

### 2.3. Single-Step Printing of HA–CHI Complex Coacervate Ink

In this paragraph, we focus on understanding the rheological features and the underlying stabilization mechanisms that render complex coacervates suitable single-step printable biomaterial inks. From all the printed complex coacervate formulations the H-L/pH6/0.15 M and H-L/pH6/0.25 M samples were identified as the most promising candidates for this purpose (Figure 2A,B). The term "single-step printable biomaterial ink" implies the following features: i) readily extrudable through a nozzle, ii) a high shape fidelity and good connectivity between the printed strands (layer adhesion), iii) cytocompatibility, and importantly, iv) no post-printing processing to solidify the designed structure. To comply with the cytocompatibility requirement and to provide a cell friendly environment, the choice was made to focus on the H-L/pH6/0.15 M sample that exhibits a NaCl concentration close to the one of the physiological conditions. The complete rheological characterization of the H-L/pH6/0.15 M sample is presented in **Figure 3**A–C.

First, the shear-thinning behavior of the ink was studied and evidenced by a drop in viscosity at shear rates above 0.1 s$^{-1}$ (Figure 3A). Shear-thinning is an important feature of biomaterials used for printing as they ideally should be extruded from a nozzle without the need of very high pressures. The theoretical shear rate experienced in the nozzle (250 μm diameter) by

**ADVANCED
SCIENCE NEWS**

www.advancedsciencenews.com

**ADVANCED
MATERIALS**

www.advmat.de

**Figure 3.** Single-step printing of HA–CHI complex coacervate ink. Rheological characterization of the H-L/pH6/0.15 M ink: A) steady-shear viscosity measurement ($\dot{\gamma} = 0.001$–$10$ s$^{-1}$); B) recovery after failure test (three cycles of $\gamma = 1\%$ for 300 s/100% for 300 s/1% for 300 s, at $\omega = 1$ rad s$^{-1}$); C) frequency sweep measurements ($\omega = 0.1$ to 100 rad s$^{-1}$, $\gamma = 1\%$ strain) of the native sample (black symbols) and of the same sample but previously extruded in air through a 0.25 mm nozzle (red symbols). D) Pictures of a 4-layer square mesh scaffold (i) and a 3D square pyramid structure (15 layers) (ii) of the HA–CHI H-L/pH6/0.15 M sample printed in air. E) Evolution of the distance between the strands of the square mesh over 60 min at rest in air. The camera pictures on which the image analysis was performed can be found in Figure S7 (Supporting Information).

H-L/pH6/0.15 M system was calculated to be ≈650 s$^{-1}$ (Figure S3A and see Supporting Information) which is much higher than the accessible shear rate with our rheometer but confidently lies in a range of shear rates for which the viscosity is low enough to assure easy extrudability of the ink. Second, by performing a recovery after failure measurement, the capability of the ink to quickly self-heal was assessed (Figure 3B). The material was subjected to low strain (1%) to imitate its state at rest, to high strain (100%) to promote its rupture ($G'' > G'$) and to low strain again. After the material was subjected to a high enough strain, the original material's storage and loss moduli were fully recovered in <10 s. The experimental data showed that the H-L/pH6/0.15 M HA–CHI ink could restore its original properties (i.e., $G'$ and $G''$) after printing, but was also able to heal, assuring reliable layer adhesion between the scaffold strands. Third, we hypothesized that the discrepancy between the high shape fidelity of the H-L/pH6/0.15 M scaffold (Figure 2B) and the short relaxation time of ≈30 s (Figures 1B and 3C, "native") is due to dehydration of the ink during printing. To verify this, a frequency sweep experiment was performed on the ink after it was subjected to an ex-

trusion procedure in air through an identical nozzle as used for printing (Figure 3C, "extruded in air"). In these conditions, the material shows a drastic slowdown of the dynamics compared to the native sample: for the extruded sample both $G'$ and $G''$ are significantly higher than for the native sample and $G'$ exceeds the $G''$ on the whole range of frequencies investigated. It is also important to note that the flow through the nozzle did not promote any additional interactions, that is, shear-induced association, that could also slow down the dynamics of the system (Figure S4, Supporting Information). These observations support the hypothesis that water evaporates from the complex coacervate during printing. The relatively high surface-to-volume ratio enables fast dehydration and renders the shape fidelity of the scaffolds very high as confirmed by the fast shrinkage of the printed strands in air (≈30% decrease of the original diameter within 5 min, Figure S5A,B, Supporting Information). Altogether, these features allowed for the successful printing of a 4-layer square mesh (Figure 3D-i), but also of a more sophisticated and challenging 3D 15-layer square pyramid structure that did not flow under its own weight upon or after printing (Figure 3D-ii).
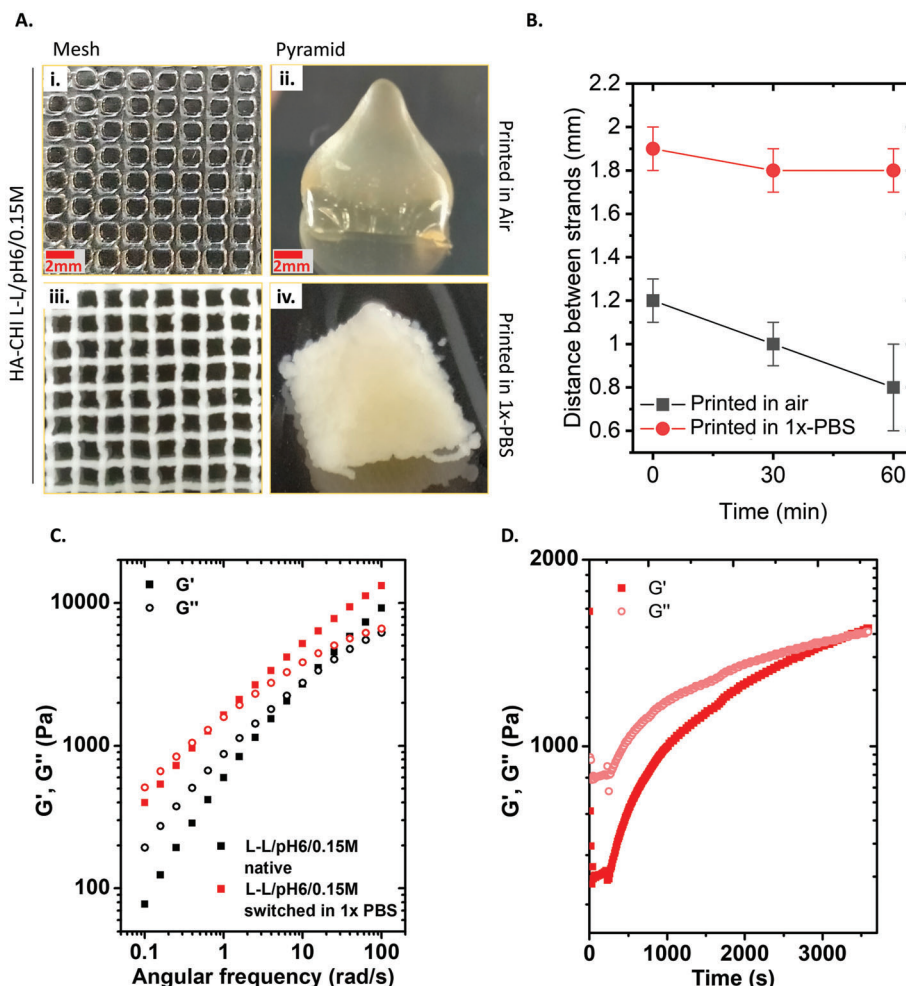
**Figure 4.** Printing complex coacervate inks in water. A) Pictures of a 4-layer square mesh scaffold (i,iii) and a 3D square pyramid structure (15-layers) (ii,iv) of the HA–CHI, L-L/pH6/0.15 M sample printed in air (i,ii) or directly in 1×-PBS buffer (iii,iv). B) Evolution of the distance between strands of the square mesh for 60 min, when kept at rest in air or in 1×-PBS bath. The camera pictures on which the image analysis was performed can be found in Figure S7 (Supporting Information). C,D) Rheological characterization of the L-L/pH6/0.15 M ink by frequency sweep ($\omega = 0.1$ to 100 rad s$^{-1}$, $\gamma = 1\%$ strain) before and after immersion in 1×-PBS (C) and time sweep ($\omega = 1$ rad s$^{-1}$, $\gamma = 1\%$ strain) upon immersion in 1×-PBS buffer (D).

Finally, the dimensional stability of the 4-layer square mesh scaffold was quantitatively determined by measuring the distance between the strands after printing in air at fixed time intervals (Figure 3E; Figures S6 and S7A, Supporting Information). In a time span of 60 min, it is observed that the 2 mm inter-strand distance decreased slightly to 1.8 mm, evidencing that shape relaxation of the printed structure is largely absent. Interestingly, after 60 min, the scaffold was dry and tough enough to be detached from the substrate and handled with tweezers (Figure S7B, Supporting Information). Moreover, single dried strands could even be knotted without breaking, showing that they are also highly flexible after drying (Figure S7C, Supporting Information).

## 2.4. Printing of HA–CHI Complex Coacervate Ink in an Aqueous Bath

After successful printing in air, in this section, we use the unique ability that complex coacervates can transition from a viscoelastic fluid to a microporous solid upon an environmental trigger, for example, by switching from higher to lower salt concentration or a change in pH.[36,38,53] We investigate the possibility of broadening the range of printable HA–CHI materials, by printing directly in water the inks that showed poor shape fidelity in air. To this end, we use the HA–CHI L-L/pH6/0.15 M ink, with a composition that is close-to-physiological conditions, and which present good shear-thinning properties (Figure S3B,C, Supporting Information), but a poor shape fidelity upon printing in air (average Pr value of 0.8: see **Figure** 4A-i,ii). The distance between the strands of the square mesh (Figure 4A-i), measured directly after printing, was ≈1.2 mm, which is 40% lower than the designed distance of 2 mm (Figure 4B; Figures S5 and S8, Supporting Information). Sixty minutes after printing, the distance between strands decreased further, reaching ≈0.85 mm (58% of the designed distance). The relatively fast relaxation rate (below 1 s) did not allow for long-term stability (Figure 4C). In the second run, the ink was printed directly into a 1×-PBS bath at pH 7.4, containing mainly [NaCl] = 0.137 M and [Na$_2$HPO$_4$] + [NaH$_2$PO$_4$] =
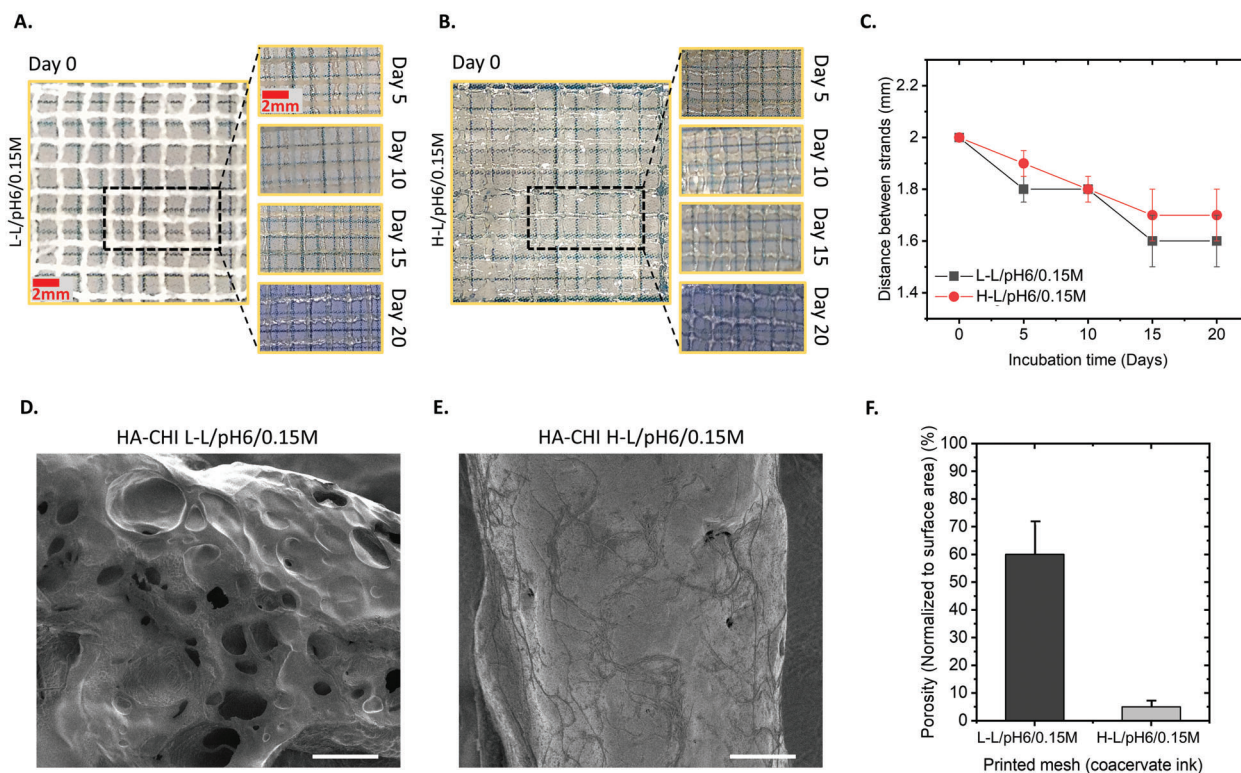
**Figure 5.** Dimensional stability, degradation, and morphology of printed scaffolds. Shape retention of the printed complex-coacervate-based inks incubated in 1×-PBS, at 37 °C, 5% $CO_2$, for a period of 20 days. A) Shape retention of the L-L/pH6/0.15 M ink directly printed in 1×-PBS and B) shape retention of H-L/pH6/0.15 M printed in air. C) Evolution of the distance between strands within the 4-layer square mesh printed scaffolds for 20 days. D,E) Cryo-SEM images of the 1×-PBS L-L/pH6/0.15 M (D) and air-printed H-L/pH6/0.15 M (E) scaffolds. Scale bars: 100 µm. F) Average surface porosity of the two printed scaffolds. See also Supporting Information for more details on the calculation of the porosity percentage.
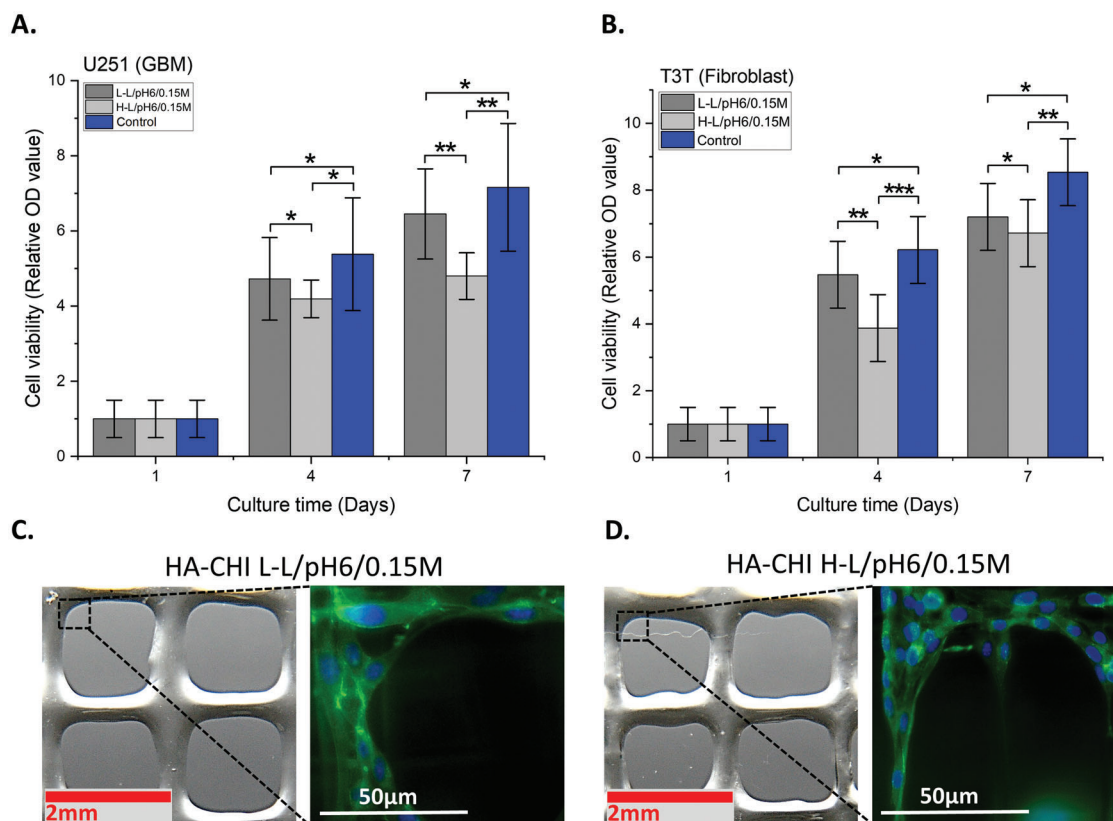
0.01 M. This time, a high shape fidelity was obtained with a distance between strands of 1.9–1.8 mm and an average Pr value close to 1.1 (60 min after printing), see Figure 4A-iii,iv,B and Figure S8 (Supporting Information). Importantly, a satisfactory adhesion between the layers was observed as no disintegration of the consecutive printed layers was noticed. Upon printing, the ink immediately turned white, indicating changes in the microscopic structure of the material, probably due to formation of microscopic pores that are able to scatter light when embedded in a polymer–water matrix.[36]

The liquid-to-solid transition experienced by the L-L/pH6/0.15 M ink was followed over time with rheology at a given frequency ($\omega = 1$ rad s$^{-1}$) (Figure 4D). Upon addition of 1×-PBS, both $G'$ and $G''$ started increasing immediately, and after 3000 s, the storage modulus value exceeded the loss modulus. The time scale of the transition probed by rheology is longer than the one observed during printing due to the low surface-to-volume ratio of the sample squeezed between the top and bottom plates of the rheometer compared to the sample printed into thin strands in the 1×-PBS medium.[36] The slowdown of the ink dynamics after immersion, and hence a better shape fidelity, is also evidenced by the shift of the crossover frequency of the moduli to a lower frequency (Figure 4C). Upon immersion in 1×-PBS, the sample experiences both a pH switch (from pH 6 to 7.4) and a change in ionic composition. As discussed previously, a higher pH was shown to decrease the dynamics of the formed HA–CHI complex coacervate. Despite the low charge density on the CHI

chains at pH 7.4 (ionization degree ≈10%, Figure S1, Supporting Information), the concomitant increase of the density of intra- and intermolecular H-bonding between CHI chains drastically slows down the chain dynamics in the printed scaffold and increases the stiffness of the resulting material. In addition, we speculate that the kosmotropic behavior of the phosphate ions in PBS has a non-neglectable impact on the chain dynamics also by decreasing the hydration of the chains.[54] Segregative phase separation of CHI chains in the complex coacervate is anticipated even to a greater extent than is observed at pH 6 and may also lead to the whitening of the printed scaffold.[47,50,51] However, this would have to be confirmed with further experiments. In conclusion, it was shown that complex coacervate inks can be solidified by simply printing directly in a 1×-PBS buffer. Indeed, an ink that was not suitable to print complex geometries in air, could be instead printed in aqueous medium. This solidification approach opens up the possibility of printing the ink directly into the cell culture medium, thereby immediately providing cell growth conditions.

## 2.5. Dimensional Stability and Degradation of the Printed Scaffolds

Then, the dimensional stability and the degradation of the two samples a priori considered as the best fit for cell studies, namely the one printed in 1×-PBS (L-L/pH6/0.15 M) and the one printed

**ADVANCED
SCIENCE NEWS**

www.advancedsciencenews.com

**ADVANCED
MATERIALS**

www.advmat.de

**Figure 6.** Cytocompatibility studies of the printed scaffolds. Cell culture studies using the meshes printed in air (H-L/pH6/0.15 M) and in 1×-PBS (L-L/pH6/0.15 M). A) Evaluation of cell viability/cytotoxicity using U251 (Glioblastoma) cell line. B) Evaluation of cell viability/cytotoxicity using 3T3 (Fibroblast) cell line. A significant difference in statistics was considered as $^{*}p \leq 0.05$; $^{**}p \leq 0.01$; $^{***}p \leq 0.001$. C) F-Actin staining (U251 cells) directly on the printed meshes after 7 days of cell culture (L-L/pH6/0.15 M). D) F-Actin staining of the U251 cells cultured directly on the printed meshes after 7 days of cell culture (H-L/pH6/0.15 M).

in air (H-L/pH6/0.15 M), were investigated in 1×-PBS physiological buffer by measuring the strand-to-strand distance using microscopy images (**Figure** 5A–C). Both the L-L/pH6/0.15 M and the H-L/pH6/0.15 M scaffolds showed a gradual decrease of the average distance between strands up to 15 days after immersion in 1×-PBS buffer before reaching a plateau. The extent of shape relaxation was limited to ≈15% for the H-L/pH6/0.15 M sample and 20% for L-L/pH6/0.15 M. Moreover, as illustrated in the insets of Figures 5A,B, the square shape of the meshes was fully maintained for both types of scaffolds, highlighting the high shape stability over time. In addition, the amount of polymer chains released in the 1×-PBS incubation solution was measured by capillary viscometry. Only ≈9 wt.% of the chains composing the scaffolds were measured to be released within the incubation medium over a 10 days' period for both the L-L/pH6/0.15 M and H-L/pH6/0.15 M samples (Figure S9, Supporting Information). The high shape stability of the printed scaffolds together with the low degradation rate represent the high durability of the complex coacervate scaffolds under incubation conditions. This shows the potential of the proposed inks to fabricate scaffolds for long term cell culture studies.

In addition, the microscopic structure of the printed scaffolds was investigated via cryo-SEM imaging (Figure 5D; Figure S10, Supporting Information). As can be seen in Figure 5D, the scaffold printed directly in 1×-PBS exhibited a porous surface (surface porosity of 60 ± 5%), in contrast to the air-printed scaffold that exhibited a relatively smooth surface (surface porosity of 8 ± 2%) (Figure 5E). More information on the calculation of the porosity percentage can be found in the Supporting Information. The porosity arises from the change in pH as well as the change in ionic composition experienced upon printing in the 1×-PBS solution that acts as a non-solvent for the complex coacervate. This leads to a drastic slowdown in the complex coacervate dynamics, preventing the release of excess water that eventually gets accumulated into microscopic pockets.[39,55,56] On the other hand, scaffolds printed in air and immersed in 1×-PBS afterward show low porosity as compared to the scaffolds printed in water. This difference can probably be explained by the fact that, when printed in air, the scaffold only dehydrates without a change in environmental conditions. The loss of water and densification of the system prevents further pore formation.

## 2.6. Cytocompatibility of the HA–CHI Complex-Coacervates-Based Printed Scaffolds

Finally, cytocompatibility of the chosen scaffolds was examined by determining their ability to support cell growth of two different

cell lines. U251 glioblastoma cells (cancer cells), known for their sensitivity and responsiveness to HA, and 3T3 mouse fibroblasts as healthy cells representative, were used.[40] The viability of cells cultured on the 1×-PBS- and air-printed scaffolds was investigated with a PrestoBlue assay upon post-printing cell seeding. A PrestoBlue assay works based on the conversion of resazurin to fluorescent resorufin by healthy cells, that can be quantitatively detected, indicating their metabolic activity. As presented in **Figure 6**A,B, both cell lines showed similar activity on control substrates, that is, Petri dishes. The two cell lines were also able to proliferate on both scaffold types over a period of 7 days, as indicated by an increase in the relative optical density value (OD), with only a slight decrease compared to the controls, indicating a high compatibility of the cells with the materials. A functional scaffold should also facilitate the interactions between the cell and the scaffold. As can be seen in Figure 6C,D, F-actin polymerization was detected in cells adhered to both air-printed and PBS-printed scaffolds, indicating active cell–ECM interactions. The cells acquired well-spread morphology, following the fibers direction. In summary, both printed scaffolds show high cytocompatibility and low cytotoxicity to support cell proliferation and spreading.

## 3. Conclusion

The present study reports the use of complex coacervates as a new class of biomaterial inks for 3D bioprinting, using hyaluronic acid (HA) and chitosan (CHI) as an example. Complex coacervates demonstrate some key advantages for 3D bioprinting: i) water-immiscible nature ensuring stability of the scaffolds; ii) tunable viscosity and cohesive properties through modulation of the non-covalent interactions between the oppositely charged polymers; iii) flexibility to use different naturally derived, unmodified and cytocompatible polyelectrolytes; iv) pore formation upon solidification in a water bath; and v) water-based nature providing a cell-friendly environment. The printability of the ink and the shape fidelity of the scaffolds are highly tunable by changes in the salt concentration, the pH and the molecular weight of the polymers. These three design parameters are known to influence: 1) the strength and dynamics of the electrostatic interactions between HA (negatively charged) and CHI (positively charged) chains; 2) the density of additional intermolecular H-bonds interactions and the water content; and 3) the density of physical chain entanglements, respectively. By adjusting the physicochemical parameters, an optimized formulation (H-L/pH6/0.15 м) was developed, exhibiting shear-thinning behavior, fast self-healing, slow relaxation dynamics at rest (due to partial dehydration once extruded), and long-term structural stability. In addition, a poorly air-printable ink formulation (L-L/pH6/0.15 м) was turned into a stable microporous scaffold by printing directly in 1×-PBS buffer. This feature is beneficial in tissue engineering applications as it enables direct printing within the cell culture medium and creates pores, thereby providing space for cell growth, nutrient and waste exchange and microvasculature formation. Additionally, both inks reveal cytocompatibility and supported cell proliferation and spreading.

## Supporting Information

Supporting Information is available from the Wiley Online Library or from the author.

## Conflict of Interest

The authors declare no conflict of interest.

## Author Contributions

M.Ko. and J.E.S. both contributed to this work equally and therefore shared the first authorship. M.Ko., M.O., M.Ka., M.K.W.-B., and J.E.S. designed the experiments. M.Ko., P.D., and J.E.S. performed pilot experiments. M.O., J.E.S., and A.A. performed the final experiments and generated all the printing data, rheological testing, and degradation analysis. J.E.S., M.O., and D.P. processed all the rheological testing data. M.Ko. and D.L. processed the printing data, shape retention test, and performed the cell culture experiments. M.Ko., M.Ka., M.K.W.-B., and J.E.S. wrote the manuscript. P.v.R., F.K., and M.Ka. supervised and funded the project. P.v.R., F.K., M.K.W.-B., and M.Ka. reviewed the paper for final preparation.

## Data Availability Statement

The data that support the findings of this study are available from the corresponding author upon reasonable request.

[1] I. Matai, G. Kaur, A. Seyedsalehi, A. McClinton, C. T. Laurencin, *Biomaterials* **2020**, *226*, 119536.

[2] A. Schwab, R. Levato, M. D'Este, S. Piluso, D. Eglin, J. Malda, *Chem. Rev.* **2020**, *120*, 11028.

[3] M. E. Cooke, D. H. Rosenzweig, *APL Bioeng.* **2021**, *5*, 011502.

[4] M. Hirsch, A. Charlet, E. Amstad, *Adv. Funct. Mater.* **2021**, *31*, 2005929.

[5] J. E. Sayed, M. Khoonkari, M. Oggioni, P. Perrin, N. Sanson, M. Kamperman, M. K. Włodarczyk-Biegun, *Adv. Funct. Mater.* **2022**.

[6] K. Markstedt, A. Escalante, G. Toriz, P. Gatenholm, *ACS Appl. Mater. Interfaces* **2017**, *9*, 40878.

[7] X. Zhang, M. Morits, C. Jonkergouw, A. Ora, J. J. Valle-Delgado, M. Farooq, R. Ajdary, S. Huan, M. Linder, O. Rojas, M. H. Sipponen, M. Osterberg, *Biomacromolecules* **2020**, *21*, 1875.

[8] J. Li, C. Wu, P. K. Chu, M. Gelinsky, *Mater. Sci. Eng.: R: Rep.* **2020**, *140*.

[9] L. Ouyang, J. P. K. Armstrong, Y. Lin1, J. P. Wojciechowski, C. Lee-Reeves, D. Hachim, K. Zhou, J. A. Burdick, M. M. Stevens, *Sci. Adv.* **2020**, *6*, eabc5529.

[10] E. Mueller, I. Poulin, W. J. Bodnaryk, T. Hoare, *Biomacromolecules* **2022**, *23*, 619.

[11] F. L. C. Morgan, L. Moroni, M. B. Baker, *Adv. Healthcare Mater.* **2020**, *9*, 1901798.

[12] S. Seiffert, J. Sprakel, *Chem. Soc. Rev.* **2012**, *41*, 909.

[13] J. Hazur, R. Detsch, E. Karakaya, J. Kaschta, J. Tessmar, D. Schneidereit, O. Friedrich, D. W. Schubert, A. R. Boccaccini, *Biofabrication* **2020**, *12*, 045004.

[14] L. Valot, J. Martinez, A. Mehdi, G. Subra, *Chem. Soc. Rev.* **2019**, *48*, 4049.

[15] J. Cha, P. Kim, *Front. Mater.* **2017**, *4*, 45.

[16] F. Ruedinger, A. Lavrentieva, C. Blume, I. Pepelanova, T. Scheper, *Appl. Microbiol. Biotechnol.* **2015**, *99*, 623.

[17] R. Raman, R. Langer, *Adv. Mater.* **2020**, *32*, 1901969.

[18] P. Mohammadi, A. S. Aranko, L. Lemetti, Z. Cenev, Q. Zhou, S. Virtanen, C. P. Landowski, M. Penttilä, W. J. Fischer, W. Wagermaier, M. B. Linder, *Commun Biol* **2018**, *1*, 86.

[19] A. Baer, S. Hänsch, G. Mayer, M. J. Harrington, S. Schmidt, *Biomacromolecules* **2018**, *19*, 4034.

[20] A. D. Malay, T. Suzuki, T. Katashima, N. Kono, K. Arakawa, K. Numata, *Sci. Adv.* **2020**, *6*, eabb6030.

[21] R. J. Stewart, C. S. Wang, H. Shao, *Adv. Colloid Interface Sci.* **2011**, *167*, 85.

[22] J. B. Addison, N. N. Ashton, W. S. Weber, R. J. Stewart, G. P. Holland, J. L. Yarger, *Biomacromolecules* **2013**, *14*, 1140.

[23] C. E. Sing, S. L. Perry, *Soft Matter* **2020**, *16*, 2885.

[24] J. van der Gucht, E. Spruijt, M. Lemmers, M. A. Cohen Stuart, *J. Colloid Interface Sci.* **2011**, *361*, 407.

[25] H. C. Lau, S. Jeong, A. Kim, *Int. J. Biol. Macromol.* **2018**, *117*, 427.

[26] A. B. Kayitmazer, A. F. Koksal, E. Kilic Iyilik, *Soft Matter* **2015**, *11*, 8605.

[27] L. Mao, Q. Pan, F. Yuan, Y. Gao, *Food Chem.* **2019**, *276*, 307.

[28] J. J. Water, M. M. Schack, A. Velazquez-Campoy, M. J. Maltesen, M. van de Weert, L. Jorgensen, *Eur. J. Pharm. Biopharm.* **2014**, *88*, 325.

[29] W. C. Blocher, S. L. Perry, *Wiley Interdiscip. Rev.: Nanomed. Nanobiotechnol.* **2017**, *9*, e1442.

[30] Q. Wang, J. B. Schlenoff, *Macromolecules* **2014**, *47*, 3108.

[31] E. Spruijt, M. A. Cohen Stuart, J. van der Gucht, *Macromolecules* **2013**, *46*, 1633.

[32] J. Sun, S. L. Perry, J. D. Schiffman, *Biomacromolecules* **2019**, *20*, 4191.

[33] R. F. Shamoun, A. Reisch, J. B. Schlenoff, *Adv. Funct. Mater.* **2012**, *22*, 1923.

[34] X. Meng, Y. Du, Y. Liu, E. B. Coughlin, S. L. Perry, J. D. Schiffman, *Macromolecules* **2021**, *54*, 5033.

[35] M. Dompé, F. J. Cedano-Serrano, O. Heckert, N. van den Heuvel, J. van der Gucht, Y. Tran, D. Hourdet, C. Creton, M. Kamperman, *Adv. Mater.* **2019**, *31*, 1808179.

[36] M. Dompé, F. J. Cedano-Serrano, M. Vahdati, L. Westerveld, D. Hourdet, C. Creton, J. der Gucht, T. Kodger, M. Kamperman, *Adv. Mater. Interfaces* **2020**, *7*, 1901565.

[37] M. Vahdati, F. J. Cedano-Serrano, C. Creton, D. Hourdet, *ACS Appl. Polym. Mater.* **2020**, *2*, 3397.

[38] T. P. Huynh, Y. Chen, F. L. Bach-Gansmo, J. Dehli, V. N. Ibsen, M. Foss, A. S. Tvilum, A. N. Zelikin, H. Birkedal, *Adv. Mater. Interfaces* **2022**, *10*, 2201491.

[39] E. N. Durmaz, M. I. Baig, J. D. Willott, W. M. de Vos, *ACS Appl. Polym. Mater.* **2020**, *2*, 2612.

[40] K. J. Wolf, J. Chen, J. Coombes, M. K. Aghi, S. Kumar, *Nat. Rev. Mater.* **2019**, *4*, 651.

[41] J. A. Burdick, G. D. Prestwich, *Adv. Mater.* **2011**, *23*, H41.

[42] M. Rinaudo, *Progress Polym. Sci.* **2006**, *31*, 603.

[43] O. Karabiyik Acar, A. B. Kayitmazer, G. Torun Kose, *Biomacromolecules* **2018**, *19*, 1198.

[44] A. E. Erickson, S. K. Lan Levengood, J. Sun, F. C. Chang, M. Zhang, *Adv. Healthcare Mater.* **2018**, *7*, 1800295.

[45] Y. Liu, C. F. Santa Chalarca, R. N. Carmean, R. A. Olson, J. Madinya, B. S. Sumerlin, C. E. Sing, T. Emrick, S. L. Perry, *Macromolecules* **2020**, *53*, 7851.

[46] B. Yu, P. M. Rauscher, N. E. Jackson, A. M. Rumyantsev, J. J. de Pablo, *ACS Macro Lett.* **2020**, *9*, 1318.

[47] L. Li, S. Srivastava, S. Meng, J. M. Ting, M. V. Tirrell, *Macromolecules* **2020**, *53*, 7835.

[48] Y. Chen, M. Yang, S. A. Shaheen, J. B. Schlenoff, *Macromolecules* **2021**, *54*, 7890.

[49] G. Lalevée, L. David, A. Montembault, K. Blanchard, J. Meadows, S. Malaise, A. Crépet, I. Grillo, I. Morfin, T. Delair, G. Sudre, *Soft Matter* **2017**, *13*, 6594.

[50] U. Lappan, B. Wiesner, U. Scheler, *Macromolecules* **2016**, *49*, 8616.

[51] M. Tekaat, D. Butergerds, M. Schonhoff, A. Fery, C. Cramer, *Phys. Chem. Chem. Phys.* **2015**, *17*, 22552.

[52] J. Sun, J. D. Schiffman, S. L. Perry, *ACS Appl. Polym. Mater.* **2022**, *4*, 1617.

[53] M. Dompé, F. J. Cedano-Serrano, M. Vahdati, U. Sidoli, O. Heckert, A. Synytska, D. Hourdet, C. Creton, J. van der Gucht, T. Kodger, M. Kamperman, *Int. J. Mol. Sci.* **2019**, *21*, 100.

[54] P. Mohammadi, C. Jonkergouw, G. Beaune, P. Engelhardt, A. Kamada, J. V. I. Timonen, T. P. J. Knowles, M. Penttila, M. B. Linder, *J. Colloid Interface Sci.* **2020**, *560*, 149.

[55] K. Murakawa, D. R. King, T. Sun, H. Guo, T. Kurokawa, J. P. Gong, *J. Mater. Chem. B* **2019**, *7*, 5296.

[56] E. N. Durmaz, J. D. Willott, A. Fatima, W. M. de Vos, *Eur. Polym. J.* **2020**, *139*, 110015.

**2210769 (11 of 11)**